

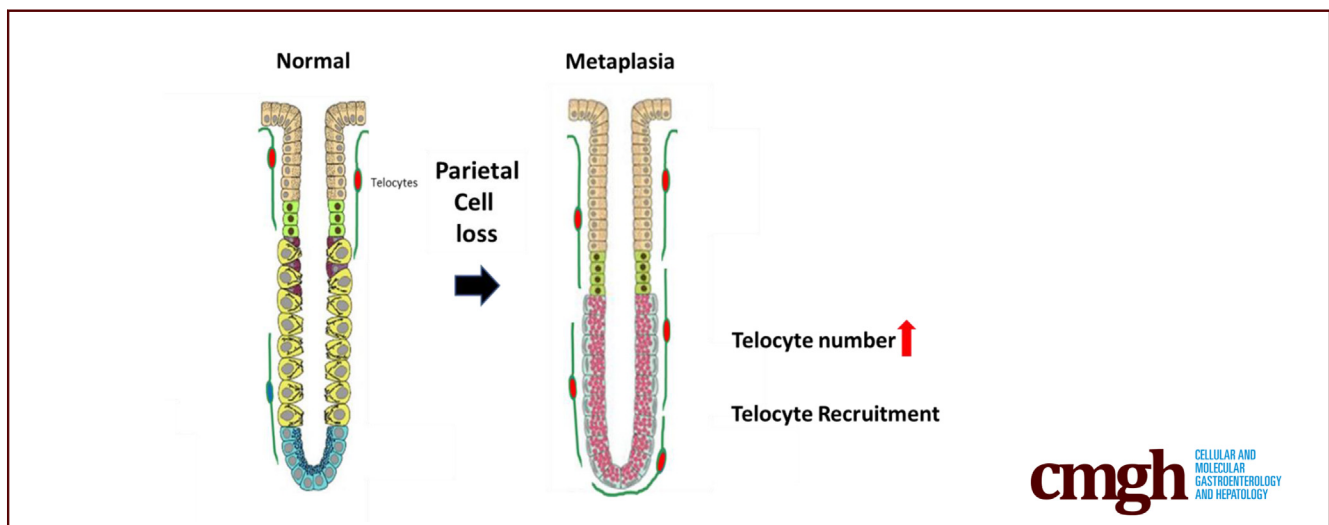
## ORIGINAL RESEARCH

## Telocyte Recruitment During the Emergence of a Metaplastic Niche in the Stomach



Yoojin Sohn,<sup>1,2,3</sup> Blake Flores Semyonov,<sup>4</sup> Hilana El-Mekkoussi,<sup>5</sup>  
Christopher V. E. Wright,<sup>1,2,3,6</sup> Klaus H. Kaestner,<sup>5</sup> Eunyoung Choi,<sup>1,2,3,4,6</sup> and  
James R. Goldenring<sup>1,2,3,4,7</sup>

<sup>1</sup>Department of Cell and Developmental Biology, Vanderbilt University School of Medicine, Nashville, Tennessee; <sup>2</sup>Vanderbilt Program in Developmental Biology, Vanderbilt University School of Medicine, Nashville, Tennessee; <sup>3</sup>Epithelial Biology Center, Vanderbilt University Medical Center, Nashville, Tennessee; <sup>4</sup>Section of Surgical Sciences, Vanderbilt University Medical Center, Nashville, Tennessee; <sup>5</sup>Department of Genetics and Center for Molecular Studies in Digestive and Liver Diseases, Perelman School of Medicine, University of Pennsylvania, Philadelphia, Pennsylvania; <sup>6</sup>Vanderbilt Center for Stem Cell Biology, Vanderbilt University School of Medicine, Nashville, Tennessee; and <sup>7</sup>Nashville VA Medical Center, Nashville, Tennessee



## SUMMARY

We sought to elucidate the role of telocytes in the development of metaplasia in mouse stomach. As metaplasia developed, the FoxL1-positive telocyte population expanded to the bases of glands, suggesting that telocytes contribute to the evolution of the metaplastic niche.

**BACKGROUND & AIM:** Telocytes, a recently identified type of subepithelial interstitial cell, have garnered attention for their potential roles in tissue homeostasis and repair. However, their contribution to gastric metaplasia remains unexplored. This study elucidates the role of telocytes in the development of metaplasia within the gastric environment.

**METHODS:** To investigate the presence and behavior of telocytes during metaplastic transitions, we used drug-induced acute injury models (using DMP-777 or L635) and a genetically engineered mouse model (Mist1-Kras). Lineage tracing via the *Foxl1-CreERT2;R26R-tdTomato* mouse model was used to

track telocyte migratory dynamics. Immunofluorescence staining was used to identify telocyte markers and evaluate their correlation with metaplasia-related changes.

**RESULTS:** We confirmed the existence of FOXL1+/PDGFR $\alpha$ + double-positive telocytes in the stomach's isthmus region. As metaplasia developed, we observed a marked increase in the telocyte population. The distribution of telocytes expanded beyond the isthmus to encompass the entire gland and closely reflected the expansion of the proliferative cell zone. Rather than a general response to mucosal damage, the shift in telocyte distribution was associated with the establishment of a metaplastic cell niche at the gland base. Furthermore, lineage-tracing experiments highlighted the active recruitment of telocytes to the emerging metaplastic cell niche, and we observed expression of *Wnt5a*, *Bmp4*, and *Bmp7* in PDGFR $\alpha$ + telocytes.

**CONCLUSIONS:** These results suggest that telocytes contribute to the evolution of a gastric metaplasia niche. The dynamic behavior of these stromal cells, their responsiveness to metaplastic changes, and potential association with *Wnt5a*, *Bmp4*, and *Bmp7* signaling emphasize the significance of telocytes in

tissue adaptation and repair. (*Cell Mol Gastroenterol Hepatol* 2024;18:■-■; <https://doi.org/10.1016/j.jcmgh.2024.04.004>)

**Keywords:** Telocyte; fibroblast; SPEM; PDGFRA; FOXL1; metaplasia; oxyntic; atrophy; WNT5A; BMP4; BMP7.

**T**elocytes are a novel type of interstitial cell found in the connective tissues of various organs, including the reproductive system, urinary system, respiratory system, cardiovascular system, and gastrointestinal tract.<sup>1,2</sup> Since their initial description in 2010,<sup>1</sup> telocytes have attracted considerable interest because of their potential roles in tissue homeostasis and regeneration. Telocytes have distinct structural characteristics with small cell bodies and long, thin cytoplasmic extensions called telopodes. Over the years, several telocyte markers have been identified, revealing that telocytes exhibit immunophenotypic heterogeneity that varies depending on their specific anatomic location.<sup>3,4</sup>

One intriguing aspect of telocytes is their potential role in tissue regeneration and repair. The mechanism by which telocytes contribute to tissue repair is not fully understood. However, it has been proposed that telocytes are involved in cell-to-cell communication, signal transmission, and maintaining tissue structure and function during wound healing.<sup>5</sup> Telocytes are involved in liver tissue regeneration, because murine models of partial hepatectomy induce an increase in their numbers.<sup>6</sup> Telocytes contribute to the formation of the extracellular matrix and the secretion of growth factors, cytokines, and chemokines, which are crucial in tissue repair.<sup>7-9</sup> Studies investigating telocytes in the gastrointestinal tract have demonstrated that, in the small and large intestines, telocytes express the winged-helix transcription factor forkhead box L1 (FOXL1) and platelet-derived growth factor receptor alpha (PDGFR $\alpha$ ).<sup>10</sup> Intestinal FOXL1-positive subepithelial telocytes form a continuous plexus just beneath the epithelial cells, and express subsets of various Wnt signaling molecules and R-spondin3 in a location-dependent manner along crypt-villus axis.<sup>10,11</sup> These intestinal telocytes function as a crucial component of the intestinal stem cell niche.

Metaplasia is defined as a conversion of 1 mature cell type to another mature cell type. In the gastrointestinal tract, metaplasia develops in response to physical or chemical damage to the mucosa. As a barrier separating the external and internal environments, the gastrointestinal mucosae promptly respond to mucosal damage by undergoing metaplasia, which serves to provide protection and facilitate tissue repair.<sup>12</sup> Reparative metaplasia is beneficial following severe injury, but this normal cellular response can become problematic in the presence of persistent damage and chronic inflammation, subsequently increasing the risk of cancer development.<sup>13</sup>

In the stomach, metaplasia develops in the setting of acute or chronic gastritis. The gastric chief cells at the base of the oxyntic glands are characterized by expression of secretory zymogens. These cells differentiate from mucous neck cells without cell division and maintain their fully differentiated state under normal circumstances,<sup>14-16</sup>

although some chief cell self-renewal may accrue over time.<sup>17</sup> When stomach acid-secreting parietal cells are lost, chief cells undergo transdifferentiation into a state of mucous cell metaplasia, referred to as spasmolytic polypeptide-expressing metaplasia (SPEM), and under continued damage and inflammation, these cells become proliferative.<sup>18,19</sup> SPEM is considered a precursor lineage for the development of intestinal metaplasia, and both of these metaplasias are possible precursor lesions for gastric cancer.<sup>20,21</sup> Earlier studies have highlighted the involvement of immune cells, including M2 macrophages and type 2 innate lymphoid cells, in the process of chief cell transdifferentiation into SPEM cells.<sup>22,23</sup> Still, the contribution of telocytes during metaplasia development remains unexplored.

In this study, we investigate the involvement of telocytes in metaplasia development within the gastric context. Our investigations not only verified the presence of FOXL1+/PDGFR $\alpha$ + double-positive telocytes in the stomach, but also uncovered their distributional dynamics in response to metaplastic transitions. In acute injury models and genetically engineered mouse models, we observed an increase in telocyte abundance during metaplasia development, accompanied by a shift in distribution from the isthmus to the base of the gland. Importantly, this altered distribution correlated with expansion of the proliferative cell zone, suggesting a connection between the telocytes and the emerging metaplastic cell niche. This dynamic migration was demonstrated using a lineage tracing approach, highlighting the adaptability and responsiveness of these stromal cells. In addition, we demonstrated the presence of *Wnt5a*, *Bmp4*, and *Bmp7* expression in PDGFR $\alpha$ -positive telocytes. These observations underscore the intricate interplay between stromal components and metaplastic changes and suggest potential molecular pathways through which telocytes could influence metaplasia development and maintenance.


## Results

### *Telocytes in the Stomach Express FOXL1 and PDGFR $\alpha$*

Leveraging the insights from prior research, our study aimed to extend the investigation of telocyte function to the stomach. Although previous research has explored telocytes within the stomach's muscle layer,<sup>2,24</sup> our objective was to investigate the potential interaction between telocytes and epithelial cells.

First, we evaluated the existence and characteristics of telocytes within the normal mouse stomach. Immunofluorescence staining was performed to investigate the

**Abbreviations used in this paper:** FOXL1, factor forkhead box L1; IL, interleukin; PBS, phosphate-buffered saline; PDGFR $\alpha$ , platelet-derived growth factor receptor alpha; SPEM, spasmolytic polypeptide-expressing metaplasia; WT, wild-type.

 Most current article

© 2024 The Authors. Published by Elsevier Inc. on behalf of the AGA Institute. This is an open access article under the CC BY-NC-ND license (<http://creativecommons.org/licenses/by-nc-nd/4.0/>).

2352-345X

<https://doi.org/10.1016/j.jcmgh.2024.04.004>

expression of FOXL1 and PDGFR $\alpha$  in telocytes within the small intestine, and in the corpus and antrum of the stomach (Figure 1A). As previously noted, in the small intestine, FOXL1+/PDGFR $\alpha$ + double-positive telocytes were distributed throughout crypt and villi,<sup>10,11</sup> and in the stomach, FOXL1+/PDGFR $\alpha$ + double-positive telocytes were located toward the top of the gland. PDGFR $\alpha$  staining delineated the full extent of the telopodes, whereas FOXL1 staining labeled the nuclei of the telocytes. We further examined the spatial distribution of telocytes within the stromal context relative to epithelial cells. Immunofluorescence staining for p120 catenin and PDGFR $\alpha$  demonstrated that PDGFR $\alpha$ -positive telocytes within the stroma were positioned in close proximity to epithelial cells (Figure 1B).

We next investigated the localization of FOXL1+/PDGFR $\alpha$ + double-positive telocytes in relationship to proliferative cells. Immunofluorescence staining for FOXL1, PDGFR $\alpha$ , and Ki67 demonstrated that these double-positive telocytes were positioned near proliferative progenitor cells in the isthmus of normal gastric glands (Figure 1C). In contrast, only single-positive PDGFR $\alpha$ -expressing fibroblasts were observed at the base of the gland, with a notable absence of proliferative epithelial cells in this region. It is important to note that, whereas PDGFR $\alpha$  single-positive cells were distributed throughout the gland, telocytes characterized by the double-positive expression of FOXL1 and PDGFR $\alpha$  were exclusively found near the isthmus. Our findings demonstrated the presence of telocyte populations in the normal stomach corpus in association with proliferative progenitor zones.

### *FOXL1+/PDGFR $\alpha$ + Double-Positive Telocytes Are Increased During Metaplasia Development in the Stomach*

Metaplasia develops in the stomach in the setting of acid-secreting parietal cell loss. In humans, the loss of parietal cells occurs because of chronic *Helicobacter pylori* infection.<sup>25</sup> However, the parietal cell loss triggered by *Helicobacter* infection is a gradual process that occurs over the course of years in humans and months in mice. To expedite the process of oxyntic atrophy and the development of metaplasia in the mouse stomach, we induced acute injury with drugs that specifically target parietal cells. These drugs (DMP-777 and L635) induce metaplasia within a matter of days, facilitating rapid observation of cellular changes in the stomach.<sup>18,26</sup> Mice treated with DMP-777 develop SPEM cells within 10 days, and treatment with L635 induces SPEM cells within 3 days. Through the induction of stomach damage and the promotion of reparative metaplasia development, our study aimed to explore the potential role of telocytes in this process.

Immunofluorescence staining for FOXL1+/PDGFR $\alpha$ + double-positive telocytes and SPEM cell markers (GSII and CD44v9) was conducted on stomach tissue obtained from mice treated with either DMP-777 or L635 to investigate the behavior of telocytes during metaplasia development (Figure 2A, B). In untreated stomach, FOXL1+/PDGFR $\alpha$ + double-positive telocytes were primarily situated near the

isthmus region. On treatment with DMP-777 or L635, which induced metaplasia characterized by GSII and CD44v9 expression at the base of the gland, we observed a notable increase in the number of FOXL1+/PDGFR $\alpha$ + double-positive telocytes. These telocytes were distributed extensively throughout the glands, including at their bases. The quantification demonstrated a significant increase in the number of FOXL1+/PDGFR $\alpha$ + /DAPI+ telocytes in the stomachs treated with either DMP-777 or L635, compared with the untreated stomach (Figure 2C). Along with the increase of FOXL1-positive telocytes, PDGFR $\alpha$  expression was globally increased within the stomachs treated with either DMP-777 or L635, particularly evident at the base of the glands (Figure 2A and B). These results suggest that PDGFR $\alpha$ -positive stromal cells, including telocytes, formed a continuous subepithelial network that comprehensively enveloped the metaplastic glands.

### *Telocytes Show Altered Distribution Near the Expanding Proliferative Zone in DMP-777-Treated Mouse Stomach*

Earlier research demonstrated that the ablation of FOXL1+ mesenchymal cells in the intestine disrupted the proliferation of intestinal stem cells, demonstrating that FOXL1+ telocytes constitute an essential niche component for the proliferative epithelial stem cells.<sup>10</sup> Based on this observation, we hypothesized similar functions for telocytes in the stomach during normal tissue homeostasis and in metaplasia. On inducing acute injury in the stomach and subsequent metaplasia via drug treatment, isthmal progenitor cells and SPEM cells become proliferative, contributing to the expansion of the proliferative cell zone at the base of the gastric glands.

Examination of the mouse stomach treated with DMP-777 over varying durations (1, 3, and 10 days) revealed changes in the distribution of FOXL1+/PDGFR $\alpha$ + double-positive telocytes, which closely correlated with the expanding proliferative cell zone. In untreated stomach tissue, only progenitor cells were positive for Ki67, concentrated in the upper region of the gland, specifically within the isthmus (Figure 3A). However, over the course of DMP-777 treatment, an expansion of the Ki67-positive proliferative cell zone was observed, gradually expanding toward the base of the gland, reaching its fullest extent after 10 days of DMP-777 treatment. Throughout this time, telocytes were consistently positioned in close proximity to the proliferating cell lineages.

In tandem with the expansion of proliferative cell zone, FOXL1+/PDGFR $\alpha$ + double-positive telocytes appeared to undergo migration and expansion toward the base of the gland, positioning themselves adjacent to the proliferating epithelial cells (Figure 3A). Aligned with the gradual expansion of the proliferative cell zone during metaplasia development, there was a corresponding extension of FOXL1+/PDGFR $\alpha$ + double-positive telocytes toward the mid-gland during the initial 1 and 3 days of DMP-777 treatment. By the end of the 10-day DMP-777 treatment, proliferative SPEM cells and FOXL1+/PDGFR $\alpha$ + double-

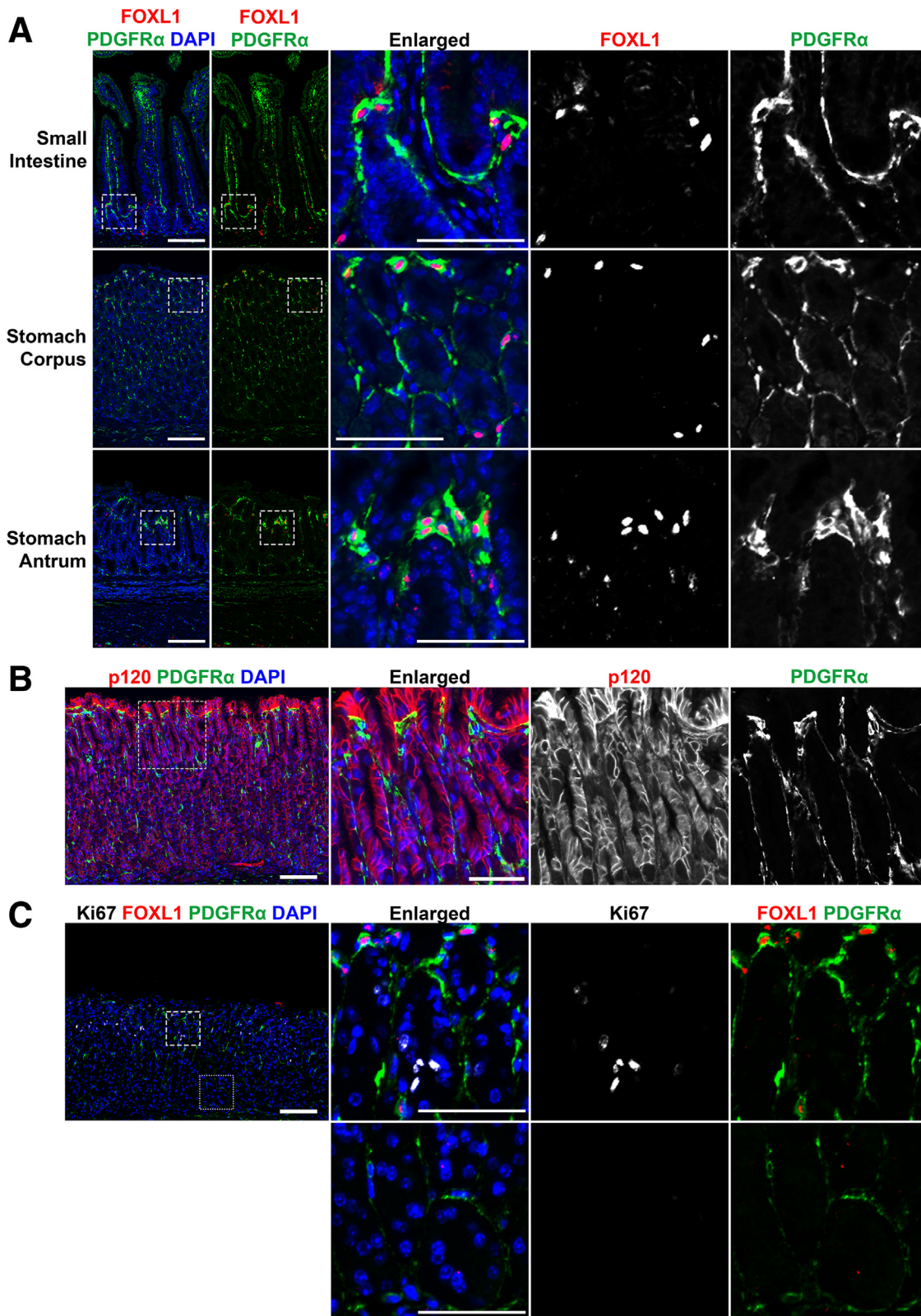


**Figure 1. Telocytes in the stomach express FOXL1 and PDGFR $\alpha$ .** (A) Immunofluorescence staining of FOXL1 (red), PDGFR $\alpha$  (green), and DAPI (blue) in the small intestine, stomach corpus, and stomach antrum. Telocytes coexpressing FOXL1 and PDGFR $\alpha$  were present in all tissues. PDGFR $\alpha$  staining revealed extended telopodes adjacent to epithelial cells, whereas FOXL1 staining marked the nuclei of telocytes. Scale bar: 100  $\mu$ m and 50  $\mu$ m for enlarged. (B) Immunofluorescence staining of p120 catenin (red), PDGFR $\alpha$  (green), and DAPI (blue). Telocytes within the stroma were positioned closely to epithelial cells. Scale bar: 100  $\mu$ m and 50  $\mu$ m for enlarged. (C) Immunofluorescence staining of Ki67 (white), FOXL1 (red), PDGFR $\alpha$  (green), and DAPI (blue). FOXL1 $^{+}$ /PDGFR $\alpha$  $^{+}$  double-positive telocytes were found near the isthmus (dashed box), where proliferative progenitor cells are located. At the gland's base (dotted box), PDGFR $\alpha$  single-positive fibroblasts were present, without proliferative cells. Scale bar: 100  $\mu$ m and 50  $\mu$ m for enlarged.

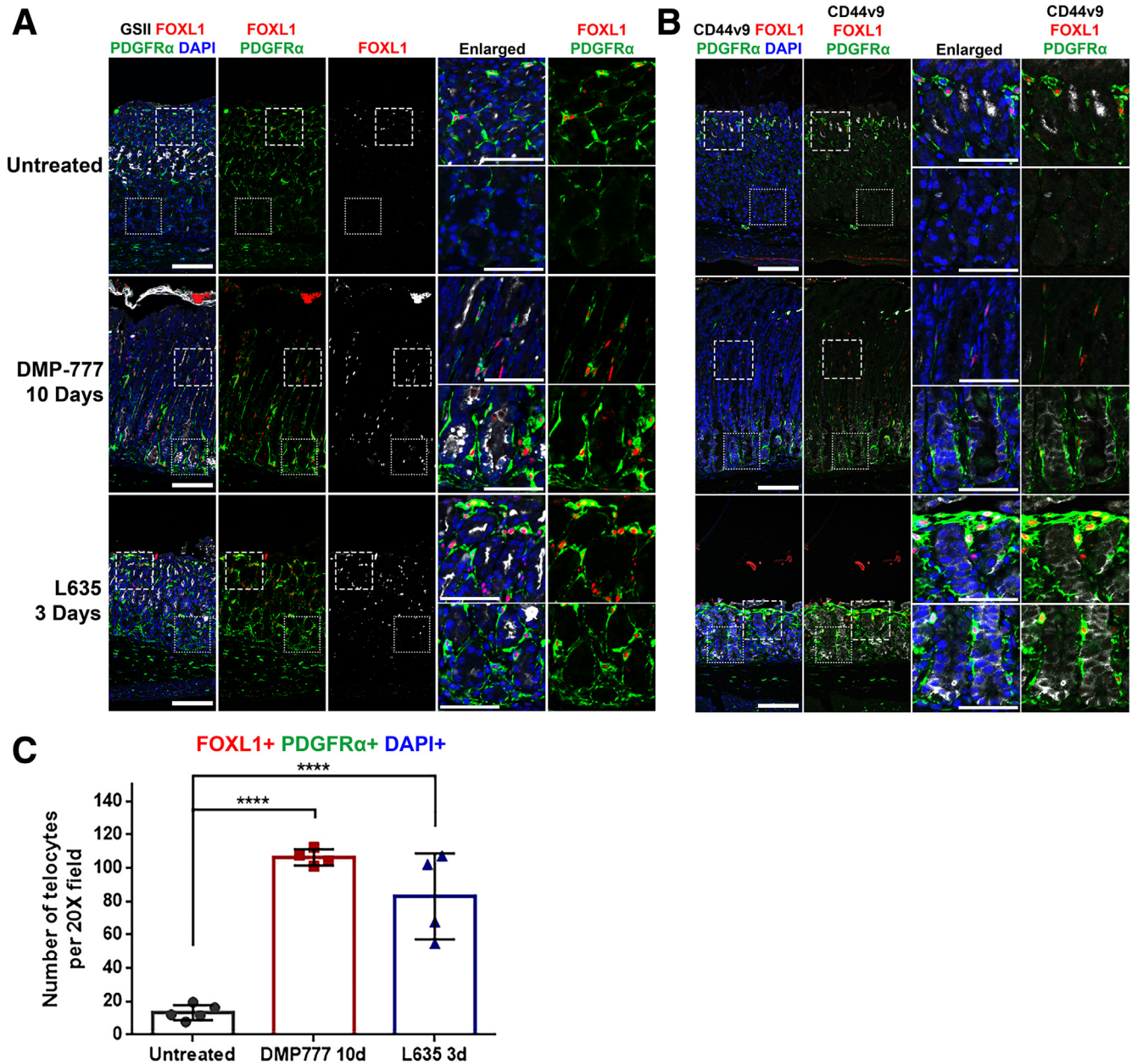


**Figure 2. FOXL1+/PDGFR $\alpha$ + double-positive telocytes are increased during the metaplasia development in the stomach.** (A) Immunofluorescence staining of GSII (white), FOXL1 (red), PDGFR $\alpha$  (green), and DAPI (blue) in DMP-777 and L635-treated mouse stomach. In untreated mouse stomach, FOXL1+/PDGFR $\alpha$ + double-positive telocytes were located near the isthmus. Following treatment with DMP-777 and L635, where metaplasia developed, there was an increase in the number of these telocytes. Also, telocytes spread throughout the gland, extending even to the base. Scale bar: 100  $\mu$ m and 50  $\mu$ m for enlarged. (B) Immunofluorescence staining of CD44v9 (white), FOXL1 (red), PDGFR $\alpha$  (green), and DAPI (blue). In the untreated stomach, FOXL1+/PDGFR $\alpha$ + double-positive telocytes were located near the isthmus. In DMP-777 and L635-treated stomach, telocytes were also observed near the CD44v9-positive metaplastic cells at the base of the gland. Scale bar: 100  $\mu$ m and 50  $\mu$ m for enlarged. (C) Quantification of telocyte count. FOXL1+/PDGFR $\alpha$ +/DAPI+ telocyte count significantly increased in DMP-777 and L635-treated stomachs. Data presented as mean  $\pm$  standard deviation (n = 5 for Untreated and n = 4 for DMP-777 and L635). \*\*\*\* $P$  < .0001. Dunnett multiple comparisons test; 1-way analysis of variance (F (2, 10) = 49.96;  $P$  < .0001).

positive telocytes were present at the very base of the gland. The quantification also demonstrated a significant increase in the number of FOXL1+/PDGFR $\alpha$ + /DAPI+ telocytes in the stomachs treated with DMP-777 (Figure 3B). These findings suggest a potential correlation between the expansion of the proliferative cell zone and the concurrent

extension of the telocyte network during the process of metaplasia development.

To gain a more comprehensive understanding of the distributional changes of the FOXL1+/PDGFR $\alpha$ + double-positive telocytes, we quantified their presence along the height of the gland, which was divided into 10% increments

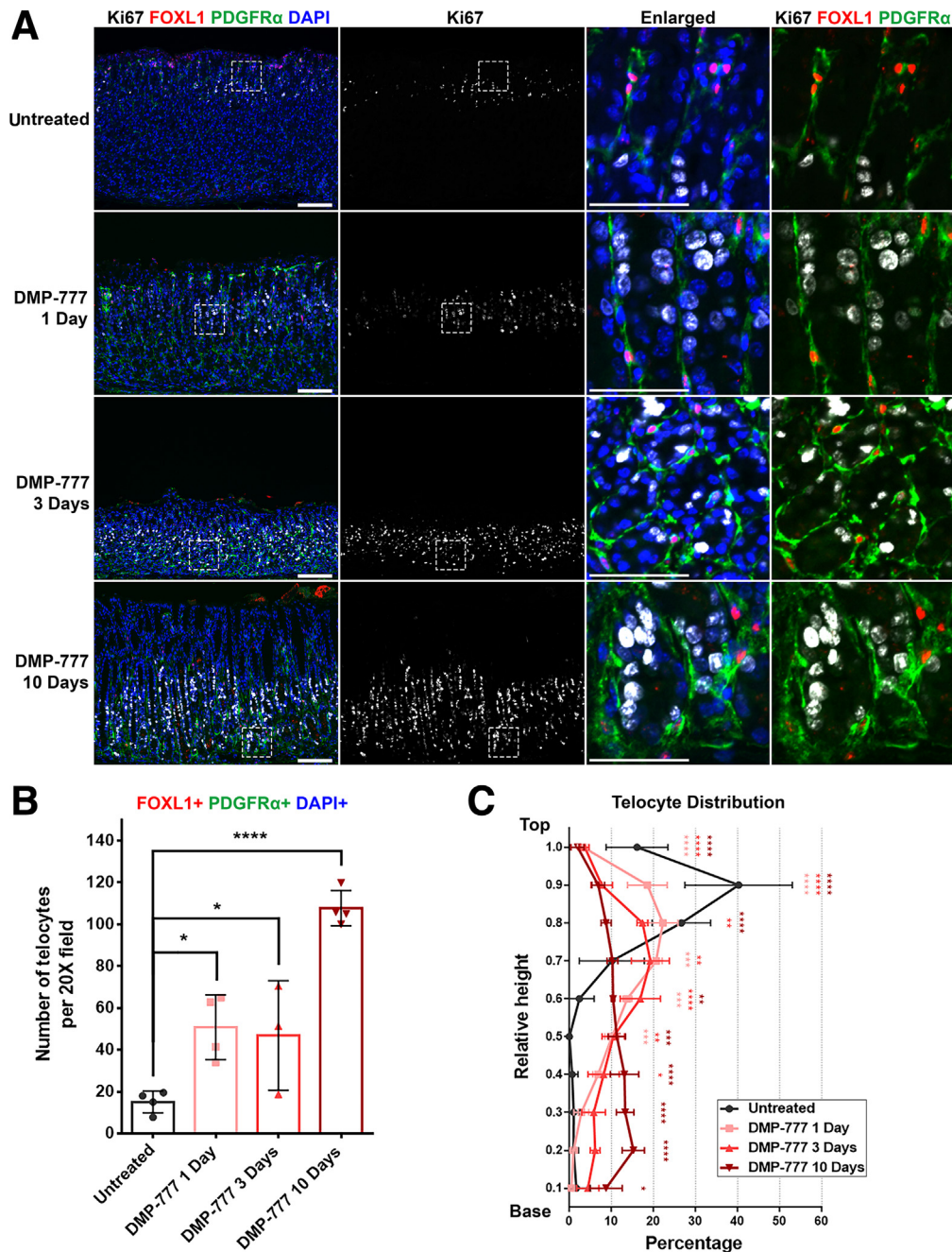


**Figure 3. Telocytes show altered distribution near the expanding proliferative zone in DMP-777-treated mouse stomach.** (A) Immunofluorescence staining of Ki67 (white), FOXL1 (red), PDGFR $\alpha$  (green), and DAPI (blue) on DMP-777-treated stomach tissue. As DMP-777 treatment duration increased, the proliferative cell zone expanded, and FOXL1+/PDGFR $\alpha$ + telocytes extended toward the base. Scale bar: 100  $\mu$ m and 50  $\mu$ m for enlarged. (B) Quantification of telocyte count. The number of FOXL1+/PDGFR $\alpha$ +/DAPI+ telocytes increased in the stomach following treatment with DMP-777. Data presented as mean  $\pm$  standard deviation (n = 4, except for DMP-777 3 Days, n = 3). \* $P$  < .05; \*\*\*\* $P$  < .0001. Dunnett multiple comparisons test; 1-way analysis of variance (F (3, 11) = 27.28;  $P$  < .0001). (C) Quantification of telocyte distribution within the gland. The distribution histograms display relative positions of FOXL1+/PDGFR $\alpha$ +/DAPI+ telocytes along the height of the gland. The y-axis represents the relative height of the corpus gland, divided into 10% increments (1 = top and 0 = base). The x-axis represents the percentage of telocytes in each region. Extended treatment with DMP-777 reduced telocyte distribution at the top and increased presence in the mid and base regions of the gland. Data presented as mean  $\pm$  standard deviation (n = 4, except for DMP-777 3 Days, n = 3). \* $P$  < .05; \*\* $P$  < .01; \*\*\* $P$  < .001; \*\*\*\* $P$  < .0001. Dunnett multiple comparisons test; 2-way analysis of variance for interaction (F (27, 99) = 15.47;  $P$  < .0001).

(1 = top and 0 = base) (Figure 3C). The analysis revealed that with the increasing duration of DMP-777 treatment, there was a progressive reduction in the distribution of telocytes within the top region of the gland. Conversely, the distribution of telocytes in the mid and base regions exhibited a significant increase. After 3 days of DMP-777 treatment, a significant increase in telocyte distribution was observed at the mid-gland region. This trend was even more pronounced after 10 days of DMP-777 treatment, with a significant increase at the base region. This observation highlighted distributional shifts of telocytes that corresponded to the expanding proliferative cell zone.

### *L635 Treatment Promotes a Shift in Telocyte Distribution Corresponding with Proliferative Zone Expansion*

To investigate the accelerated development of metaplasia within 3 days, we used another drug, L635. Immunofluorescence staining for Ki67, FOXL1, and PDGFR $\alpha$  was performed to assess the telocyte distribution in correlation with alterations in the proliferative cell zone. In untreated stomach tissue, immunofluorescence staining revealed the localization of Ki67-positive progenitor cells in the isthmus, and FOXL1+/PDGFR $\alpha$ + double-positive telocytes were also observed in close proximity to the proliferative cells. (Figure 4A). Following L635 treatment, there was an expansion of the Ki67-positive proliferative cell zone, which coincided with the extension of FOXL1+/PDGFR $\alpha$ + double-positive telocytes toward the gland's base.

The quantification demonstrated a significant increase in the number of telocytes in the stomachs treated with L635 for 3 days (Figure 4B). To further understand the distributional changes of FOXL1+/PDGFR $\alpha$ + double-positive telocytes, a quantitative analysis for telocyte distribution was conducted (Figure 4C). The results demonstrated a progressive decrease in telocyte distribution at the top region with increasing duration of L635 treatment, accompanied by a concurrent increase in their distribution at the mid and base regions. Particularly, after 3 days of L635 treatment, a significant increase in telocyte distribution at the mid and base region was observed. These observations highlight distributional shifts of telocytes that parallel the changes in the proliferative cell zone during L635 treatment.

In summary, our findings suggest that FOXL1+/PDGFR $\alpha$ + double-positive telocytes display an altered distribution pattern near the proliferative cell zone in response to acute injury induced by drug treatments. The correlation between the expansion of the proliferative cell zone and the concurrent extension of the telocyte network highlights a potential interaction between these cells during metaplasia development.

### *Telocytes Exhibit a Consistent Proximity to the Proliferative Cell Zone During Recovery*

Earlier research has already demonstrated that discontinuing DMP-777 treatment results in the reversal of the acute drug-induced injury, leading to the recovery of

changes induced by DMP-777 within 14 days after the cessation of treatment.<sup>26</sup> We next investigated the behavior of telocytes in mouse stomach tissue that had undergone recovery from DMP-777-induced injury.

On DMP-777 10 days treatment, the stomach exhibited an expanded proliferative cell zone and an extended telocyte network, as discussed previously (Figure 5A). Nevertheless, after 14 days of recovery, FOXL1+/PDGFR $\alpha$ + double-positive telocytes reverted to their normal distribution, exclusively located at the top of the gland. This reversion paralleled the restoration of the normal proliferative cell zone, marked by the presence of progenitor cells primarily situated in the isthmus.

The quantification revealed that the significant increase in the number of telocytes present in the DMP-777-treated stomach regressed postrecovery and was not significantly different from that observed in the untreated stomach (Figure 5B). DMP-777 induced a shift in telocyte distribution, resulting in their increased presence in the mid and base regions of the gastric gland (Figure 5C). However, following recovery, the distribution of telocytes reflected that in the untreated stomach, where most telocytes were localized at the top region of the gland. These findings demonstrate that FOXL1+/PDGFR $\alpha$ + double-positive telocytes consistently maintain their proximity to the proliferative cell zone during the injury caused by DMP-777 and the subsequent recovery phase, suggesting a dynamic crosstalk between telocytes and the proliferative epithelial cells during injury and healing processes.

### *Telocytes Are Increased During Kras-Driven Metaplasia Development in the Stomach*

In addition to the drug-induced acute injury mouse model, we further explored telocyte distribution using a genetically engineered mouse model known as Mist1-Kras mice. In these mice, the administration of tamoxifen triggers the expression of a constitutively active Kras allele (G12D) in Mist1-expressing chief cells, leading to the onset of metaplasia within 1 month.<sup>27</sup> This model offers a distinct mode of metaplasia development compared with acute injury, simulating the gradual changes driven by genetic modifications in chief cells.

In the wild-type (WT) control stomach, FOXL1+/PDGFR $\alpha$ + double-positive telocytes were located near the proliferative progenitor cells at the top of the gland as noted before (Figure 6A). In contrast, in the Mist1-Kras 1 month stomach, which showed prominent metaplasia development, a notable shift occurred in the FOXL1+/PDGFR $\alpha$ + double-positive telocytes. These telocytes were observed at the base of the gland, where proliferative metaplastic cells were also found. Quantitative analysis demonstrated a significant increase in the count of FOXL1+/PDGFR $\alpha$ + /DAPI+ telocytes in the Mist1-Kras metaplastic stomach (Figure 6B). Moreover, the quantitative analysis for telocyte distribution within the gland revealed a distinct redistribution pattern in the Mist1-Kras metaplastic stomach (Figure 6C). This shift was marked by

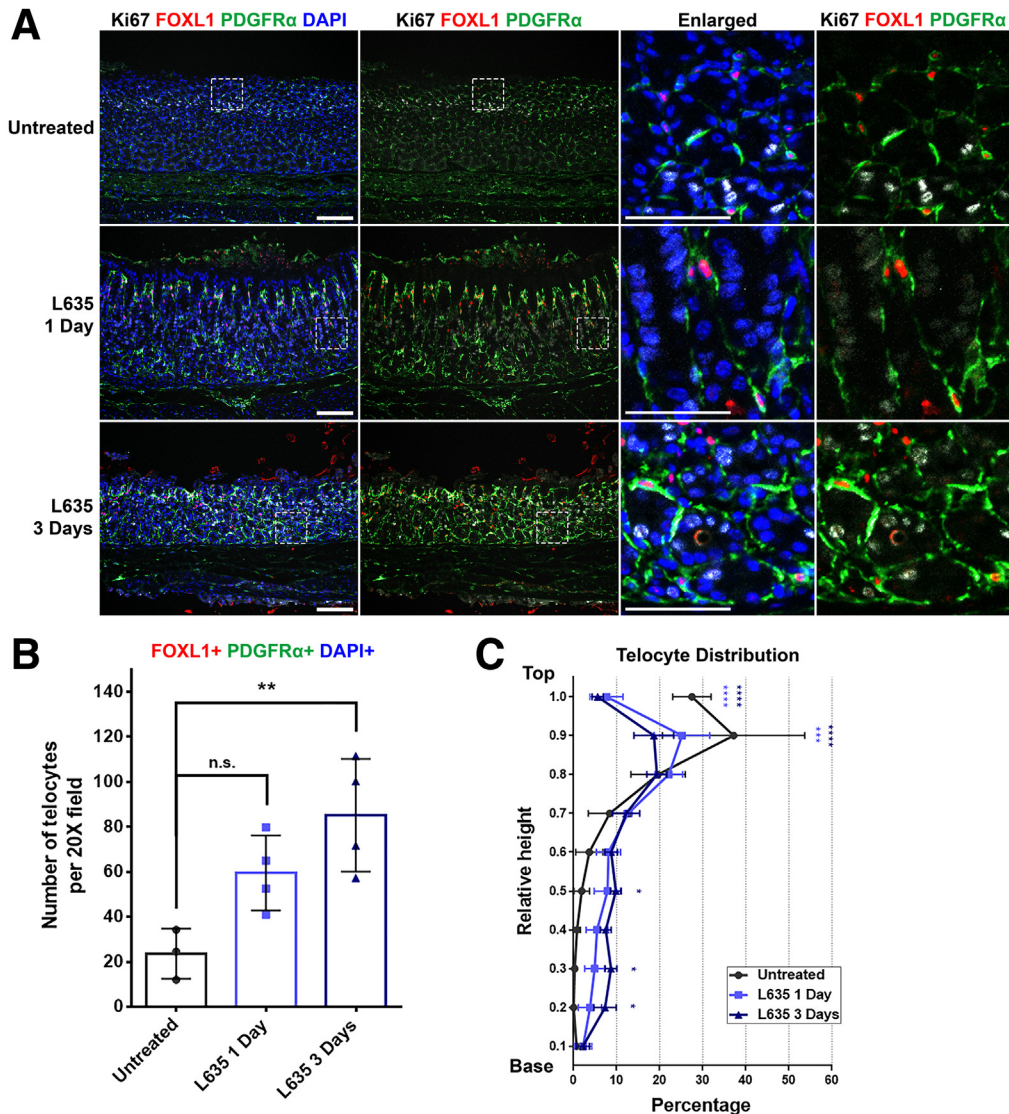


**Figure 4. L635 treatment promotes a shift in telocyte distribution corresponding with proliferative zone expansion.** (A) Immunofluorescence staining of Ki67 (white), FOXL1 (red), PDGFR $\alpha$  (green), and DAPI (blue) on L635-treated mouse stomach tissue. In untreated stomachs, Ki67-positive zone and FOXL1+/PDGFR $\alpha$ + telocytes were located in the upper region. With L635 treatment, the progenitor zone expanded, accompanied by telocytes extending toward the gland's base. Scale bar: 100  $\mu$ m and 50  $\mu$ m for enlarged. (B) Quantification of telocyte count. The number of FOXL1+/PDGFR $\alpha$ +/DAPI+ telocytes increased with L635 treatment. Data presented as mean  $\pm$  standard deviation (n = 4, except for Untreated, n = 3). n.s., not statistically significant; \*\*P < .01. Dunnett multiple comparisons test; 1-way analysis of variance (F (2, 8) = 8.777; P = .0096). (C) Quantification of telocyte distribution within the gland. Telocyte distribution is illustrated in distribution histograms, where the y-axis represents the relative height within the corpus gland, divided into 10% increments (1 = top and 0 = base), and the x-axis represents the percentage of telocytes in each region. Extended treatment with L635 reduced telocyte distribution at the top but increased their presence in the mid and base regions. Data presented as mean  $\pm$  standard deviation (n = 4, except for Untreated, n = 3). \*P < .05; \*\*\*P < .001; \*\*\*\*P < .0001. Dunnett multiple comparisons test; 2-way analysis of variance for interaction (F (18, 72) = 6.704; P < .0001).

a decrease in telocyte distribution at the top region of the gland and a concurrent increase in their abundance at the mid and base regions. In summary, our findings from Mist1-Kras mouse stomach tissue during metaplasia development demonstrated a pattern analogous to what was observed with telocytes during acute injury. Again, these findings suggest the potential for interactions between telocytes and the evolving metaplastic cell niche.

### Telocytes Are Found at the Base of the Gland Only When Metaplasia Develops

To investigate whether the observed telocyte relocation during metaplasia was solely attributed to mucosal injury or potentially associated with the establishment of a metaplastic cell niche, we used a mouse model deficient in the interleukin (IL)33 receptor (ST2), known as the ST2KO mouse model, wherein metaplasia development is



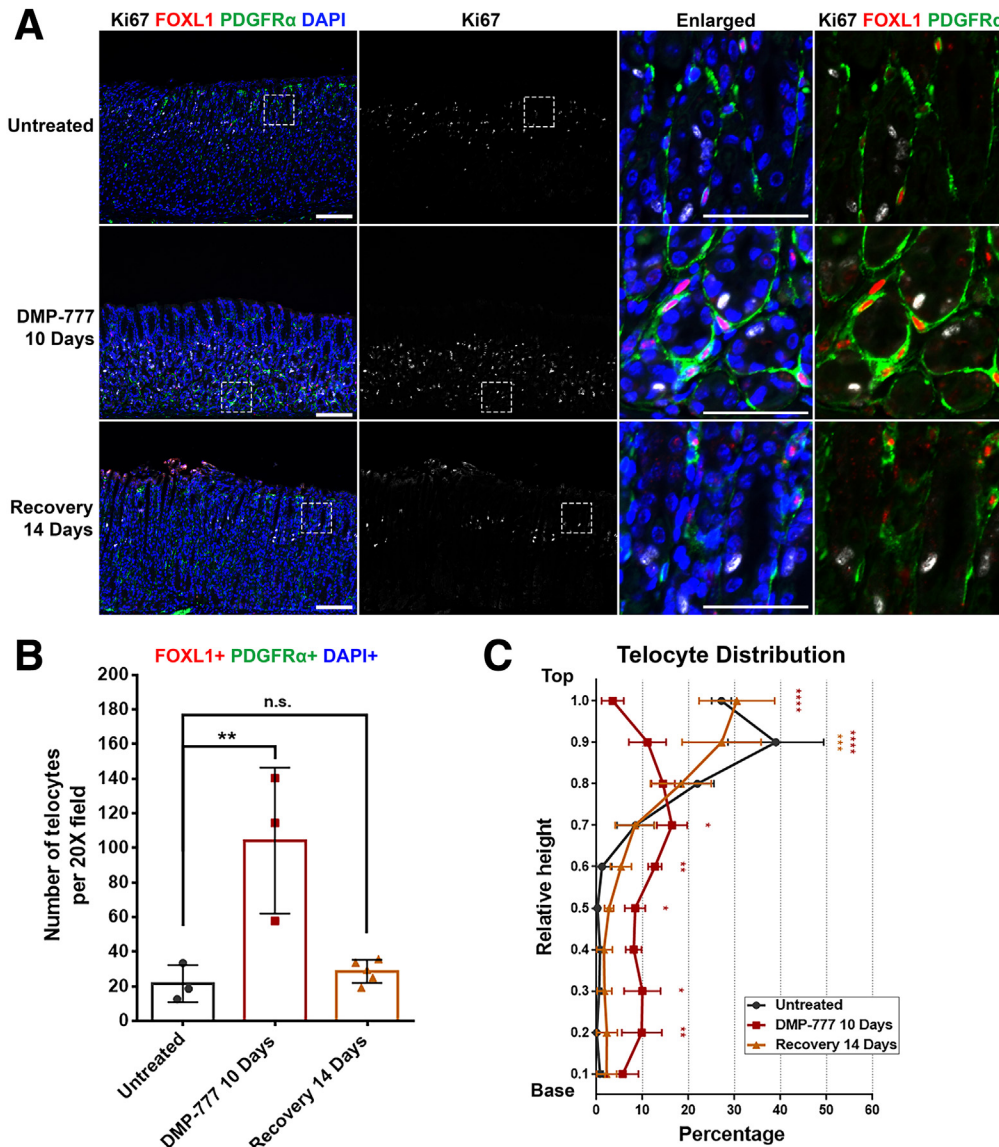


**Figure 5. Telocytes exhibit a consistent proximity to the proliferative cell zone during recovery.** (A) Immunofluorescence staining of Ki67 (white), FOXL1 (red), PDGFR $\alpha$  (green), and DAPI (blue) on recovered mouse stomach tissue following DMP-777 treatment. The injury-induced changes, including the expansion of the proliferative zone and telocyte distribution, were restored after a 14-day recovery period, with FOXL1 $^{+}$ /PDGFR $\alpha$  $^{+}$  double-positive telocytes reverting to their normal position at the isthmus. Scale bar: 100  $\mu$ m and 50  $\mu$ m for enlarged. (B) Quantification of telocyte count. The number of FOXL1 $^{+}$ /PDGFR $\alpha$  $^{+}$ /DAPI $^{+}$  telocyte was increased in DMP-777-treated stomachs. Postrecovery, the telocyte count regressed and was not significantly different from that in untreated stomach. Data presented as mean  $\pm$  standard deviation (n = 3, except for Recovery 14 days, n = 5). n.s., not statistically significant; \*\* $P$  < .01. Dunnnett multiple comparisons test; 1-way analysis of variance (F (2, 8) = 13.54;  $P$  = .0027). (C) Quantification of telocyte distribution within the gland. Telocyte distribution is illustrated in distribution histograms, where the y-axis represents the relative height within the corpus gland, divided into 10% increments (1 = top and 0 = base), and the x-axis represents the percentage of telocytes in each region. DMP-777 treatment altered telocyte distribution, increasing their presence in the mid and base regions. Postrecovery, telocyte distribution returned to a pattern similar to that observed in untreated stomachs, predominantly at the top of the gland. Data presented as mean  $\pm$  standard deviation (n = 3, except for Recovery 14 days, n = 5). \* $P$  < .05; \*\* $P$  < .01; \*\*\* $P$  < .001; \*\*\*\* $P$  < .0001. Dunnnett multiple comparisons test; 2-way analysis of variance for interaction (F (18, 72) = 10.52;  $P$  < .0001).

interrupted. In the ST2KO mouse treated with L635, chief cell transdifferentiation was stalled, preventing the emergence of proliferative metaplasia, even in the context of parietal cell loss.<sup>19</sup> Furthermore, the administration of recombinant IL13 to ST2KO mice alongside L635 treatment

resulted in the re-establishment of metaplasia in the absence of IL33 signaling.<sup>19</sup> This model provided an opportunity to dissect the relationship between mucosal injury, cellular responses, and the subsequent metaplasia development.

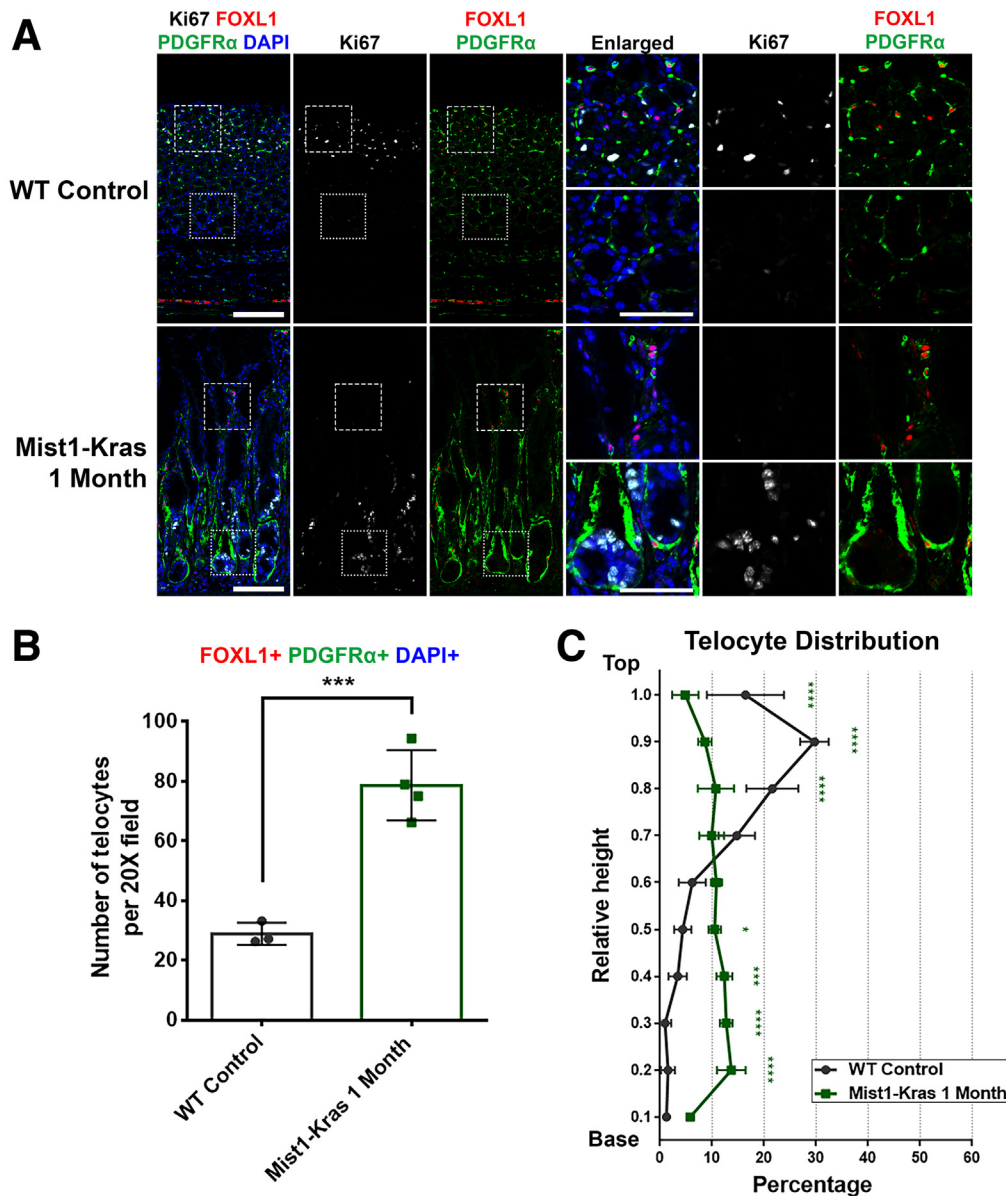


**Figure 6. Telocytes are increased during *Kras*-driven metaplasia development in the stomach.** (A) Immunofluorescence staining of Ki67 (white), FOXL1 (red), PDGFR $\alpha$  (green), and DAPI (blue) on Mist1-Kras mouse stomach tissue. In the WT control, telocytes are situated near the gland's top with proliferative progenitor cells. However, in Mist1-Kras 1-month stomach, these telocytes are detected at the base where proliferative cells accumulate. Scale bar: 100  $\mu$ m and 50  $\mu$ m for enlarged. (B) Quantification of telocyte count. The number of FOXL1+ PDGFR $\alpha$ + DAPI+ telocytes increased in Mist1-Kras metaplastic stomach. Data presented as mean  $\pm$  standard deviation (n = 3 for Untreated and n = 4 for Mist1-Kras 1 month). \*\*\**P* < .001. Unpaired *t* test. (C) Quantification of telocyte distribution within the gland. Telocyte distribution is illustrated in distribution histograms, where the y-axis represents the relative height within the corpus gland, divided into 10% increments (1 = top and 0 = base), and the x-axis represents the percentage of telocytes in each region. Mist1-Kras 1-month stomach exhibited a redistribution of telocytes, showing a reduced presence at the top and an enhanced distribution at the mid and base regions. Data presented as mean  $\pm$  standard deviation (n = 3 for Untreated and n = 4 for Mist1-Kras 1 month). \**P* < .05; \*\*\**P* < .001; \*\*\*\**P* < .0001. Dunnett multiple comparisons test; 2-way analysis of variance for interaction (F (9, 45) = 28.41; *P* < .0001).

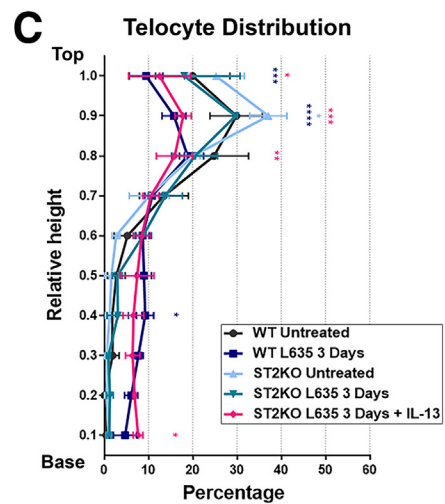
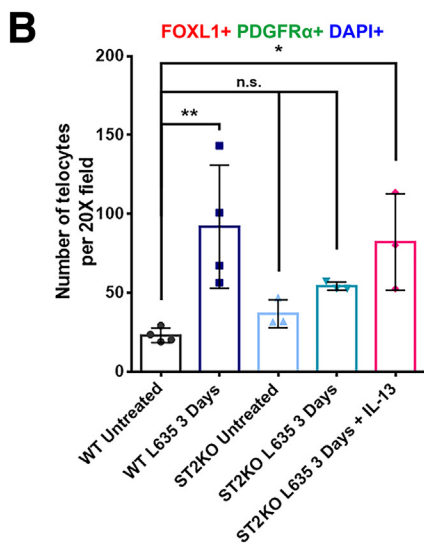
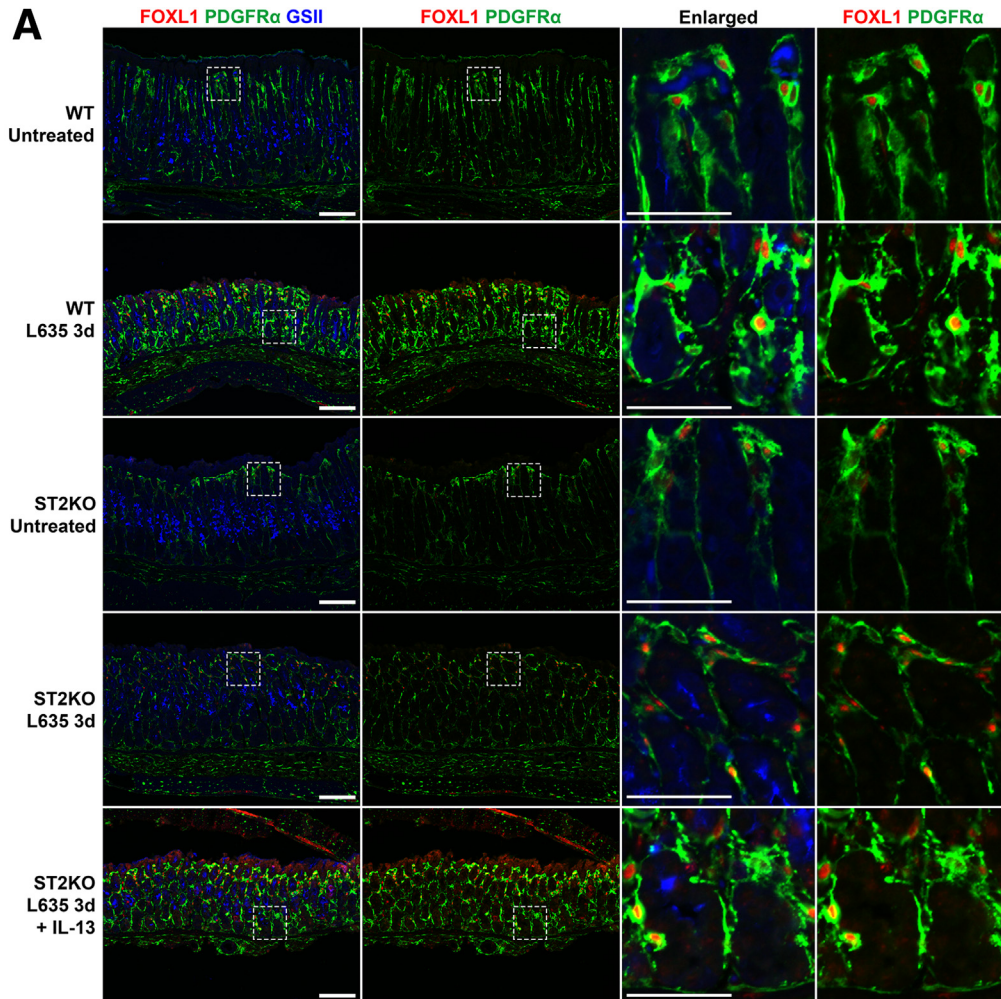
Using immunofluorescence staining for GSII, FOXL1, and PDGFR $\alpha$ , we examined the metaplasia development and telocyte distribution in the ST2KO mouse model (Figure 7A). As discussed previously, untreated stomachs predominantly displayed telocytes at the upper region, whereas telocyte extension toward the base of the gland was observed in L635-treated stomach. In untreated ST2KO stomach, the

telocyte distribution closely resembled that observed in the untreated WT stomach, with telocytes concentrated on the top region of the gland. In L635-treated ST2KO stomach, consistent with previous reports, metaplasia characterized by GSII expression at the gland's base did not manifest. Furthermore, FOXL1+/PDGFR $\alpha$ + double-positive telocytes were absent from the gland base in this context.

Nevertheless, on supplementation with recombinant IL13, metaplasia emerged at the base of the gland, coinciding with the appearance of telocytes in this region.

The quantification revealed a significant increase in the number of telocytes in WT stomach treated with L635 and

ST2KO stomach treated with both L635 and recombinant IL13, whereas ST2KO stomach and ST2KO treated L635 alone did not show a significant change in telocyte frequency (Figure 7B). Additionally, the telocyte distribution analysis was also conducted to quantitatively assess the



observed changes (Figure 7C). In ST2KO stomach treated with L635, the distribution of telocytes remained unchanged. However, a significant shift in telocyte distribution was evident when ST2KO stomach received both L635 and recombinant IL13. This redistribution was characterized by a decrease in telocytes in the top region and a simultaneous increase in their presence at the base region, replicating the changes observed during metaplasia development in L635-treated WT stomach.

These findings shed light on the complex interplay among mucosal injury, the establishment of a metaplastic cell niche, and the recruitment of telocytes during metaplasia development. Notably, the shift in telocyte distribution was specifically associated with the presence of metaplastic cells at the base, suggesting that telocyte relocation is closely tied to the establishment of a metaplastic cell niche.

### Telocytes Are Actively Recruited During Metaplasia Development

To investigate the recruitment of telocytes during the development of metaplasia in the stomach, we used the previously described inducible *Foxl1*-dependent lineage-tracing model.<sup>11</sup> *Foxl1-CreERT2* mice were crossed with *R26R-tdTomato* mice to label *Foxl1*-expressing telocytes selectively with tdTomato and subsequently traced their behavior following mucosal damage induced by L635. Our aim was to discern whether telocytes located near the more basal proliferative cell zone in metaplastic glands originated from existing telocytes situated near the isthmus in normal glands. We performed immunofluorescence staining for FOXL1, PDGFR $\alpha$ , and RFP to detect the tdTomato-labeled telocytes in *Foxl1-CreERT2;R26R-tdTomato* mouse stomach tissue. We observed tdTomato-labeled FOXL1+/PDGFR $\alpha$ + double-positive telocytes at the top of the gland in stomach tissue from mice treated only with tamoxifen, in agreement with our findings with endogenous FOXL1 immunostaining (Figure 8A). In contrast, we observed the extension of tdTomato-labeled *Foxl1*-expressing telocytes toward the base of the gland in *Foxl1-CreERT2;R26R-tdTomato* mice treated with L635. This visual evidence highlighted the recruitment of *Foxl1*-

expressing telocytes to the metaplastic niche during metaplasia development in response to injury.

For a more comprehensive understanding of the distribution and network of these labeled telocytes, we used 3-dimensional whole mount imaging coupled with tissue clearing techniques. Subsequently, 3-dimensional imaging was performed using confocal microscopy to capture the endogenous tdTomato fluorescence. The result recapitulated the distribution pattern observed in immunofluorescence staining conducted on 2-dimensional tissue sections (Figure 8B). In the context of tamoxifen-only treated stomach, the tdTomato-labeled telocytes were predominantly situated toward the upper region of the gland. However, in L635-treated stomachs, a distinct expansion of these telocytes was evident as they extended their network toward the gland's base. These telocytes exhibited elongated telopodes that projected toward the mid and base of the gland, illustrating a pronounced shift in their distribution associated with metaplasia development. We also captured orthogonal views from different planes (x/y, x/z, and y/z) to obtain additional perspectives on the altered telocyte distribution (Figure 8C). By using maximum intensity projections on orthogonal views, we enhanced the visualization of the endogenous tdTomato single-channel image. This visualization revealed that telocytes labeled by tdTomato exhibited significant elongation toward the base of the gland in the L635-treated stomach, in contrast to the tamoxifen-only control.

### *Wnt5a*, *Bmp4*, and *Bmp7* Expression in PDGFR $\alpha$ -Positive Telocytes

To gain further insights into the molecular mechanisms underlying the potential role of telocytes in metaplasia development, we directed our focus to signaling molecules expressed in intestinal telocytes (*Wnt5a*, *Bmp4*, and *Bmp7*).<sup>11</sup> Recent studies have highlighted that these WNT and BMP transcripts are enriched in a mesenchymal population characterized by the high expression of *Pdgfra* in the small intestine and the stomach.<sup>28,29</sup> Using RNA-scope fluorescence in situ hybridization, we assessed RNA expression of the signaling molecules while concurrently

**Figure 7. Telocytes are only found at the base of the gland when metaplasia develops in that region.** (A) Immunofluorescence staining of FOXL1 (red), PDGFR $\alpha$  (green), and GSII (blue) on the ST2KO mouse model. Inhibition of metaplasia development in the ST2KO stomach was observed. L635 treatment on the ST2KO stomach prevented metaplasia and resulted in the absence of telocytes at the base. However, supplementation with recombinant IL13 induced metaplasia and concurrent telocyte presence. The untreated ST2KO stomach exhibited telocyte distribution similar to the untreated WT stomach. Scale bar: 100  $\mu$ m and 50  $\mu$ m for enlarged. (B) Quantification of telocyte count. The number of FOXL1+ PDGFR $\alpha$ + DAPI+ telocytes did not change in ST2KO untreated or ST2KO L635-treated stomachs. However, there was a significant increase in the number of telocytes in ST2KO treated with both L635 and recombinant IL13. Data presented as mean  $\pm$  standard deviation (n = 4 for WT and n = 3 for ST2KO). n.s., not statistically significant; \**P* < .05; \*\**P* < .01. Dunnett multiple comparisons test; 1-way analysis of variance (F (4, 12) = 5.682; *P* = .0084). (C) Quantification of telocyte distribution within the gland. Telocyte distribution is illustrated in distribution histograms, where the y-axis represents the relative height within the corpus gland, divided into 10% increments (1 = top and 0 = base), and the x-axis represents the percentage of telocytes in each region. Administration of L635 in ST2KO mice resulted in an unchanged telocyte distribution. However, combined treatment L635 and recombinant IL13 in ST2KO mice led to a shift in telocyte distribution, characterized by a reduction of telocytes at the top and an increase of telocytes at the base. Data presented as mean  $\pm$  standard deviation (n = 3 for Untreated and n = 4 for Mist1-Kras 1 month). \**P* < .05; \*\**P* < .01; \*\*\**P* < .001; \*\*\*\**P* < .0001. Dunnett multiple comparisons test; 2-way analysis of variance for interaction (F (36, 108) = 4.932; *P* < .0001).

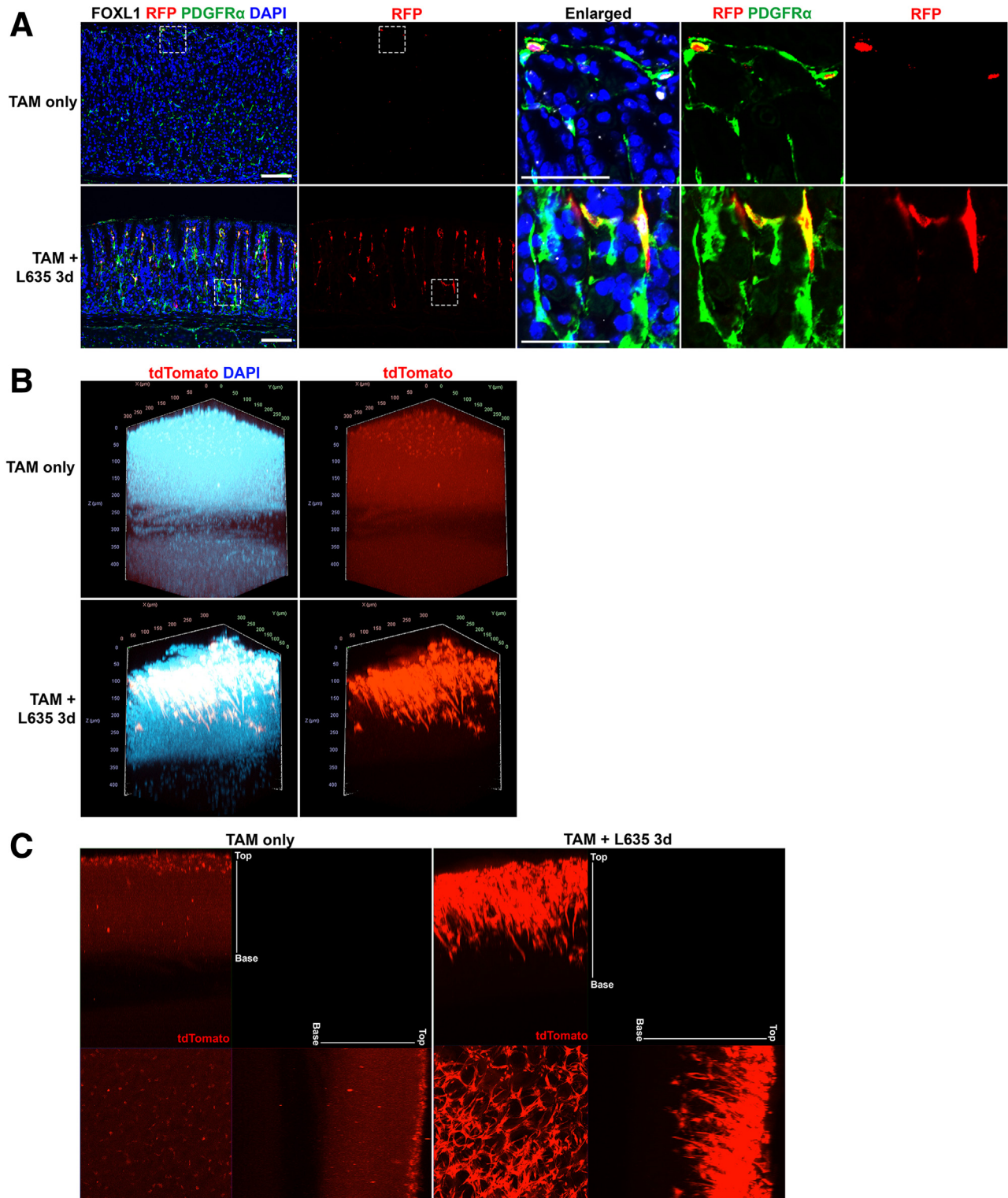


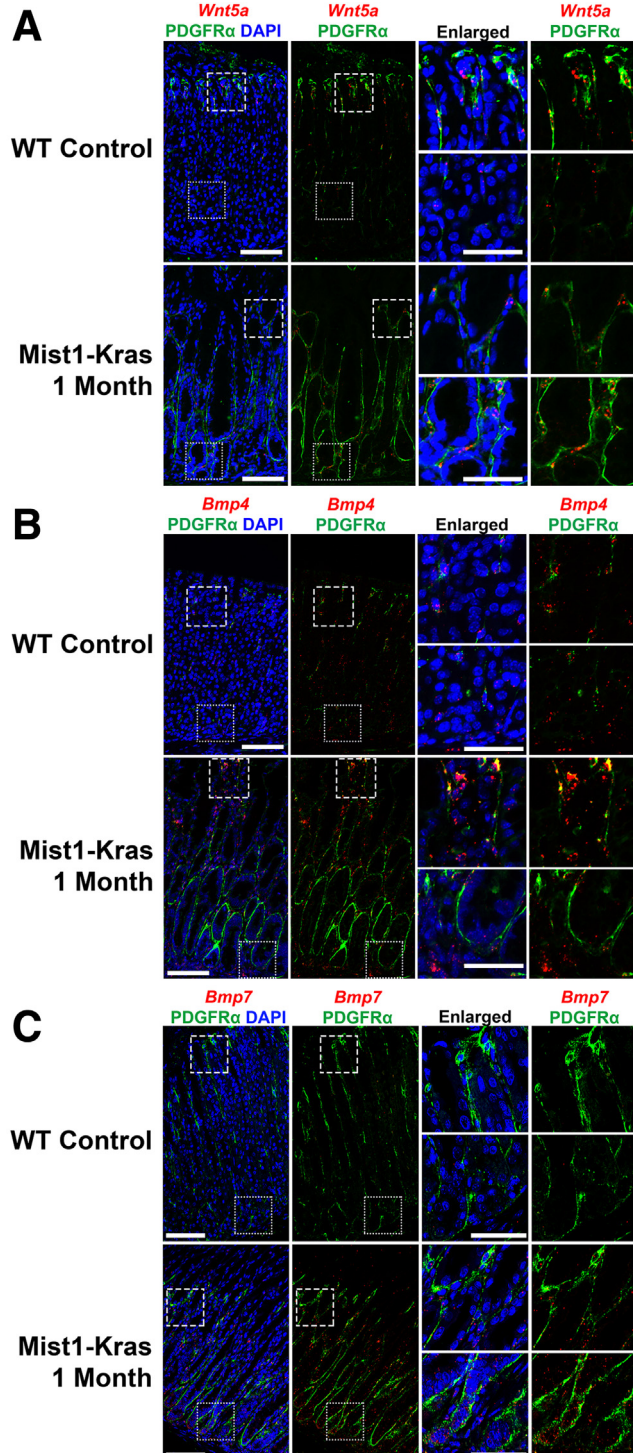
**Figure 8. Telocytes are actively recruited during metaplasia development.** (A) Immunofluorescence staining of RFP (red), FOXL1 (white), PDGFR $\alpha$  (green), and DAPI (blue) on L635-treated *Foxl1-CreERT2;R26R-tdTomato* mouse stomach tissue. The use of RFP antibody to detect the tdTomato expression revealed an extension of labeled Foxl1-expressing telocytes toward the base of the gland, specifically in L635-treated stomach tissue. Scale bar: 100  $\mu$ m and 50  $\mu$ m for enlarged. (B) Three-Dimensional whole mount image of *Foxl1-CreERT2;R26R-tdTomato* mouse stomach tissue after tissue clearing. Endogenous tdTomato (red) and DAPI (cyan) were observed under a confocal microscope. Whereas untreated stomachs mainly exhibited tdTomato-labeled telocytes at the upper part of the gland, L635 treatment showed these telocytes expanded with longer telopodes reaching the gland's mid and base sections. (C) Orthogonal views obtained from different planes (x/y, x/z and y/z) using maximum intensity projection. Endogenous tdTomato (red) signal showed telocytes in the L635-treated stomach extending further to the gland base, contrasting with the TAM-only control.

performing immunofluorescence staining for PDGFR $\alpha$  on stomach sections from Mist1-Kras mice 1 month after induction.

In the WT control stomach, *Wnt5a* expression, detected by the RNAscope fluorescence in situ hybridization, displayed a distinct enrichment within the PDGFR $\alpha$ -positive cell population, predominantly located at the upper part of the gland (Figure 9A). This specific pattern of *Wnt5a*

localization aligned with the distribution of telocytes observed in the same region. In contrast, in the context of metaplastic Mist1-Kras 1-month induced stomach, the expression of *Wnt5a* extended more broadly throughout the gland, encompassing PDGFR $\alpha$ -positive cells, which reached from the top to the base of the metaplastic glands. This shift in *Wnt5a* expression in PDGFR $\alpha$ -positive cells reflected the expanded distribution of telocytes to the base of the gland in metaplastic regions.

In the WT control stomach, *Bmp4* colocalized with PDGFR $\alpha$ -positive cells throughout the gland and was also present in PDGFR $\alpha$ -negative stromal cells (Figure 9B). In the metaplastic Mist1-Kras 1-month stomach, there was a prominent increase in *Bmp4* expression throughout the gland in PDGFR $\alpha$ -positive and other stromal cells. Thus, although telocytes may not be the sole source of *Bmp4*, there is an upregulation of *Bmp4* during metaplasia development. Similarly, although *Bmp7* was undetectable in WT stomachs, its expression markedly increased in PDGFR $\alpha$ -positive cells and epithelial cells in metaplastic tissues (Figure 9C). This observation underscores an enhanced expression of *Bmp4* and *Bmp7*, notably within telocytes associated with metaplasia.



## Discussion

The results presented in this study shed light on the role of telocytes in the stomach, especially concerning their response to mucosal injury and metaplasia development. By elucidating their recruitment, migration, and potential

**Figure 9. *Wnt5a* expression colocalizes with PDGFR $\alpha$ -positive telocytes and reflects the telocyte distribution shift in metaplasia.** (A) RNAscope fluorescence in situ hybridization of *Wnt5a* (red) and immunofluorescence staining of PDGFR $\alpha$  (green) and DAPI (blue) on Mist1-Kras 1-month mouse stomach. *Wnt5a* expression, detected by RNAscope, exhibited colocalization with PDGFR $\alpha$ -positive cells located toward the upper region of the WT control stomach, where telocytes were observed. In the metaplastic Mist1-Kras 1-month stomach, *Wnt5a* expression extended throughout the gland in PDGFR $\alpha$ -positive cells, encompassing the base of the gland. Scale bar: 100  $\mu$ m and 50  $\mu$ m for enlarged. (B) RNAscope fluorescence in situ hybridization of *Bmp4* (red) and immunofluorescence staining of PDGFR $\alpha$  (green) and DAPI (blue) on Mist1-Kras 1-month mouse stomach. In the WT control stomach, colocalization of *Bmp4* expression with PDGFR $\alpha$ -positive cells was observed throughout the gland. Additionally, *Bmp4* expression was noted in PDGFR $\alpha$ -negative cells within the stroma of the WT control stomach. In the metaplastic Mist1-Kras 1-month stomach, *Bmp4* expression was enhanced throughout the gland in both PDGFR $\alpha$ -positive cells and within the stromal compartment. Scale bar: 100  $\mu$ m and 50  $\mu$ m for enlarged. (C) RNAscope fluorescence in situ hybridization of *Bmp7* (red) and immunofluorescence staining of PDGFR $\alpha$  (green) and DAPI (blue) on Mist1-Kras 1-month mouse stomach. *Bmp7* expression was not detected in the WT control stomach. In the metaplastic Mist1-Kras 1-month stomach, a general increase in *Bmp7* expression was observed in PDGFR $\alpha$ -positive cells and epithelial cells. Scale bar: 100  $\mu$ m and 50  $\mu$ m for enlarged.

signaling contributions, we contribute to the growing understanding of the complex microenvironmental interactions that drive tissue adaptation and disease progression. Telocytes, characterized by the coexpression of FOXL1 and PDGFR $\alpha$  markers, are found in the small intestine and the stomach. Within the stomach, FOXL1+/PDGFR $\alpha$ + double-positive telocytes are predominantly located near the isthmus region where proliferative progenitor cells reside, maintaining an optimal position to function as a component of the isthmal progenitor niche, providing necessary factors to the proliferative cells.

A significant aspect of this study is that the population of FOXL1+/PDGFR $\alpha$ + double-positive telocytes increases during the development of metaplasia. This phenomenon is evident in drug-induced and genetically induced active Kras-driven metaplasia. However, telocytes did not extend toward the base of the gland in ST2KO mouse models treated with L635, where metaplasia development was arrested,<sup>19</sup> even though prominent loss of parietal cells was present. The telocytes redistributed in the ST2KO mice on supplementation with IL13, which reestablished development of metaplasia. Thus, telocyte relocation is not a generic response to mucosal injury, but may specifically function to support the establishment of a metaplastic cell niche at the gland base.

The observed increase in the number of telocytes and the expansion of the telocyte network during metaplasia development in the stomach are consistent with previous reports on the involvement of telocytes in tissue regeneration and repair in other organs, including the liver and skin.<sup>5,6</sup> Beyond simple numerical increases, these telocytes also extend their network within the metaplastic gland shifting from their initial position in the isthmus to span the entire gland down to its base. This altered distribution of telocytes coincides with the expansion of the proliferative cell zone in the stomach gland during metaplasia. The use of the *Foxl1-CreERT2;R26R-tdTomato* mouse model for lineage tracing provides insights into the elongation and migratory dynamics of the telocytes. The lineage labeling in the mice demonstrated the trajectory of labeled telocytes from their initial position in the upper glandular region to the proliferative cell zone at the gland base, indicating that the recruitment of telocytes to the metaplastic cell niche predominantly originates from preexisting telocytes in the isthmus. However, it should be noted that previous work and the present studies have identified PDGFR $\alpha$ + cells at the bases of normal glands.<sup>29</sup> In the normal mucosa, these PDGFR $\alpha$ + cells do not express FOXL1. Thus, the potential for the de novo formation of FOXL1+ telocytes from other PDGFR $\alpha$ + fibroblasts or even inflammatory fibroblasts cannot be ruled out, suggesting additional possible pathways for their formation in response to metaplasia development. Nonetheless, the recruitment of FOXL1+ telocytes to the emerging metaplastic cell niche underscores their role in facilitating or supporting the metaplasia development.

A noteworthy observation regarding this alteration in telocyte distribution during metaplasia is its resemblance to PDGFR $\alpha$ + cells in the human stomach. Recent investigations

from our group identified a population of PDGFR $\alpha$ + telocyte-like cells in the human stomach and established their involvement in gastric carcinogenesis.<sup>30</sup> Similar to telocytes, PDGFR $\alpha$ + stromal cells in the human stomach were predominantly located in the isthmus region of the normal stomach corpus, and expansion of these cells was observed in close proximity to the epithelium at the bases of metaplastic and dysplastic glands.<sup>30</sup> The consistent distribution pattern of PDGFR $\alpha$ + cells across human and mouse stomach tissues underscores the potential translational implications of insights gained from mouse models for understanding human pathology. Unfortunately, no antibody reagents are presently available for immunodetection of FOXL1 in human fixed tissue samples.

These investigations also support the integral role of gastric telocytes, particularly through the expression of secreted factors, such as *Wnt5a*, *Bmp4*, and *Bmp7*. Notably, single-cell transcriptomic analyses had revealed the expression of *WNT5A* and *BMP4* within PDGFR $\alpha$ + telocyte-like cells in human metaplastic stomach.<sup>30</sup> In the mouse stomach, the expression of *Wnt5a*, *Bmp4*, and *Bmp7* colocalizes with PDGFR $\alpha$ -positive telocytes, and their enriched expression during metaplasia reflects the shift in telocyte distribution. Given the recognized significance of Wnt and BMP signaling pathways in tissue homeostasis and regeneration, the enriched expression of *Wnt5a*, *Bmp4*, and *Bmp7* in the metaplastic stomach suggests that fibroblast populations may establish gradients of these factors in establishing a supportive niche potentially driving or maintaining the metaplastic process.

In conclusion, the findings of this study contribute to the understanding of telocyte biology in the stomach, particularly the roles of telocytes during mucosal injury and metaplasia development. These results serve as a foundation for future investigations, presenting a potential avenue to explore the functional significance of telocytes within the gastric mucosa. Further study of telocyte and fibroblast influences on mucosal lineage differentiation and maintenance could support the development of interventions targeting the progression of metaplasia-associated gastric carcinogenesis.

## Materials and Methods

### Mice

Approximately 8 weeks C57BL/6 mice were used for mouse experiments. For drug treatment experiments, DMP-777 was dissolved in 1% methylcellulose and administered through oral gavage (350 mg/kg) once a day for up to 10 consecutive days. L635 was dissolved in deionized DNA and RNA-free water and administered through oral gavage (350 mg/kg) once a day for up to 3 consecutive days. Archival sections of stomach from Mist1-Kras mice and ST2 knockout mice were obtained from previous studies.<sup>19,27</sup> The generation of *Foxl1-CreERT2* mice has been described previously.<sup>11</sup> For lineage-tracing experiments of *Foxl1*-expressing cells, *Foxl1-CreERT2* mice were crossed with *R26R-tdTomato* mice, and 5 mg tamoxifen was administered to these mice subcutaneously daily for a total of 3 doses. L635 was

then administered 7 days posttamoxifen injection, for 3 consecutive days. Regular mouse chow and water ad libitum were provided during experiments in a temperature-controlled room with 12-hour light-dark cycles. All treatment maintenance and care of animals in these studies followed protocols approved by the Institutional Animal Care and Use Committees of Vanderbilt University.

### Immunofluorescence Staining

Mouse stomachs were fixed in 4% paraformaldehyde overnight and transferred into 70% ethanol for paraffin embedding. Five-micrometer paraffin-embedded sections were used for all immunofluorescence staining. Sections were deparaffinized, rehydrated, and submitted to antigen retrieval using Target Retrieval solution (Dako North America, Inc) in a pressure cooker. Blocking was performed by using Protein Block Serum-Free (Dako North America, Inc) for 90 minutes at room temperature. The primary antibody incubation was performed in Antibody Diluent with Background Reducing Components (Dako North America, Inc) overnight at 4°C. Primary antibodies used were as follows: goat anti-PDGFR $\alpha$  (1:500; R&D systems), guinea pig anti-FOXL1 (1:1500; developed by Dr. Christopher Wright<sup>10</sup>), rat anti-Ki67 (1:200; BioLegend) and rabbit anti-Ki67 (1:1000; Cell Signaling), mouse anti-p120 catenin (1:200; BD Biosciences), and rat anti-CD44v9 (1:25,000; Cosmo Bio). Fluorescent second antibodies (1:500; Jackson ImmunoResearch) and Alexa-488 and 647-conjugated GSII (1:2000) were incubated for 1 hour at room temperature. FOXL1 staining required the use of amplification of signal using tyramide (TSA systems; PerkinElmer). After incubation with DAPI for 5 minutes, slides were mounted with ProLong Gold Antifade Reagent (Invitrogen). Fluorescence imaging was analyzed by using an Axio Imager 2 microscope (Carl Zeiss AG).

### Immunofluorescence Quantitation

Experimental groups contained 3–5 mice. Images were analyzed using CellProfiler (Cambridge, MA) to quantify objects and verified manually (nuclei, cells). At least 4 representative images (>100 glands) of proximal stomach corpus were taken from each mouse at 20x objective for quantification. Quantification of telocyte distribution within the gland was conducted by assessing their presence in 10 distinct positions along the gland's height, divided into 10% increments (1 = top and 0 = base). All graphs and statistics were generated using GraphPad Prism. Significance was determined through various methods including unpaired *t* test, 1-way analysis of variance with Dunnett multiple comparisons test, or 2-way analysis of variance with Dunnett multiple comparisons test (n.s. = not statistically significant; \**P* < .05; \*\**P* < .01; \*\*\**P* < .001; \*\*\*\**P* < .0001).

### Tissue Clearing

Tissue clearings using CUBIC protocol was performed as previously described.<sup>31</sup> Briefly, fixed tissue was dissected into small fragments and incubated in 5-mL CUBIC R1a

solution (10% urea, 5% Quadrol, 10% Triton X-100, and 25mM NaCl in distilled water) for 2 days at 37°C with shaking. The tissues were then incubated in 5-mL blocking and permeabilization solution (5% DMSO, 0.5% Triton X-100, and 2% normal donkey serum in phosphate-buffered saline [PBS]) overnight at 4°C. The tissues were washed 6 times with 0.2- $\mu$ g/mL DAPI in PBS over a 24-hour period at 4°C. The tissues were then incubated in 5-mL CUBIC R2 solution (50% sucrose, 25% urea, 10% triethanolamine, and 0.1% Triton X-100 in distilled water) for 2 days at RT with shaking. The tissues were transferred into 500- $\mu$ L RapiClear 1.52 (Sunjin Lab) to match the refractive index and incubated overnight at 4°C. The tissues were then mounted on Glass Bottom Culture Dish (MatTek Corporation) with RapiClear 1.52. The tissues were imaged using ZEISS LSM 980 with Airyscan 2 in the Vanderbilt Cell Imaging Shared Resource Core.

### RNAscope–Fluorescence In Situ Hybridization

Stomachs from WT and Mist1-Kras mice, fixed in 10% neutral buffered formalin, were used. RNAscope fluorescence in situ hybridization was performed using the RNAscope LS Multiplex Fluorescent Reagent Kit (322800, Advanced Cell Diagnostics) according to manufacturer's protocol using a Bond RX Autostainer (Vanderbilt Translational Pathology Shared Resource), except for the addition of immunofluorescence detection of PDGFR $\alpha$ . Briefly, sections were deparaffinized, treated with heat target retrieval and protease, followed by a series of hybridizations with the target-specific probes (316798, *Wnt5a*; 401301, *Bmp4*; 407901, *Bmp7*) and amplifiers. After probe detection with OPAL520 dye, sections were washed with PBS, blocked using Protein Block Serum-Free (Dako North America, Inc), and incubated with goat anti-PDGFR $\alpha$  (1:500; R&D systems) primary antibody overnight at 4°C. After washing with PBS, sections were stained with fluorescent second antibodies for 1 hour at room temperature. Sections were washed in PBS, incubated with DAPI for 5 minutes, and slides were mounted with ProLong Gold Antifade Reagent. Fluorescence imaging was analyzed by using an Axio Imager 2 microscope (Carl Zeiss AG).

## References

1. Popescu LM, Faussone-Pellegrini MS. TELOCYTES - a case of serendipity: the winding way from interstitial cells of Cajal (ICC), via interstitial Cajal-like cells (ICLC) to TELOCYTES. *J Cell Mol Med* 2010;14:729–740.
2. Rosa I, Marini M, Manetti M. Telocytes: an emerging component of stem cell niche microenvironment. *J Histochem Cytochem* 2021;69:795–818.
3. Bei Y, Wang F, Yang C, et al. Telocytes in regenerative medicine. *J Cell Mol Med* 2015;19:1441–1454.
4. Klein M, Csobonyeiova M, Danisovic L, et al. Telocytes in the female reproductive system: up-to-date knowledge, challenges and possible clinical applications. *Life (Basel)* 2022;12:267.
5. Wang L, Song D, Wei C, et al. Telocytes inhibited inflammatory factor expression and enhanced cell



- migration in LPS-induced skin wound healing models in vitro and in vivo. *J Transl Med* 2020;18:60.
6. Wang F, Song Y, Bei Y, et al. Telocytes in liver regeneration: possible roles. *J Cell Mol Med* 2014; 18:1720–1726.
  7. Pomerleau V, Nicolas VR, Jurkovic CM, et al. FOXL1+ telocytes in mouse colon orchestrate extracellular matrix biodynamics and wound repair resolution. *J Proteomics* 2023;271:104755.
  8. Albulescu R, Tanase C, Codrici E, et al. The secretome of myocardial telocytes modulates the activity of cardiac stem cells. *J Cell Mol Med* 2015;19:1783–1794.
  9. Cretoiu D, Xu J, Xiao J, et al. Telocytes and their extracellular vesicles-evidence and hypotheses. *Int J Mol Sci* 2016;17:1322.
  10. Aoki R, Shoshkes-Carmel M, Gao N, et al. Foxl1-expressing mesenchymal cells constitute the intestinal stem cell niche. *Cell Mol Gastroenterol Hepatol* 2016; 2:175–188.
  11. Shoshkes-Carmel M, Wang YJ, Wangenstein KJ, et al. Subepithelial telocytes are an important source of Wnts that supports intestinal crypts. *Nature* 2018; 557:242–246.
  12. Goldenring JR. Pyloric metaplasia, pseudopyloric metaplasia, ulcer-associated cell lineage and spasmolytic polypeptide-expressing metaplasia: reparative lineages in the gastrointestinal mucosa. *J Pathol* 2018; 245:132–137.
  13. Meyer AR, Goldenring JR. Injury, repair, inflammation and metaplasia in the stomach. *The Journal of physiology* 2018;596:3861–3867.
  14. Goldenring JR, Nam KT, Mills JC. The origin of pre-neoplastic metaplasia in the stomach: chief cells emerge from the Mist. *Exp Cell Res* 2011; 317:2759–2764.
  15. Lennerz JK, Kim SH, Oates EL, et al. The transcription factor MIST1 is a novel human gastric chief cell marker whose expression is lost in metaplasia, dysplasia, and carcinoma. *Am J Pathol* 2010;177:1514–1533.
  16. Bredemeyer AJ, Geahlen JH, Weis VG, et al. The gastric epithelial progenitor cell niche and differentiation of the zymogenic (chief) cell lineage. *Dev Biol* 2009; 325:211–224.
  17. Burclaff J, Willet SG, Saenz JB, et al. Proliferation and differentiation of gastric mucous neck and chief cells during homeostasis and injury-induced metaplasia. *Gastroenterology* 2020;158:598–609. e5.
  18. Nam KT, Lee HJ, Sousa JF, et al. Mature chief cells are cryptic progenitors for metaplasia in the stomach. *Gastroenterology* 2010;139:2028–2037. e9.
  19. Petersen CP, Meyer AR, De Salvo C, et al. A signalling cascade of IL-33 to IL-13 regulates metaplasia in the mouse stomach. *Gut* 2018;67:805–817.
  20. Schmidt PH, Lee JR, Joshi V, et al. Identification of a metaplastic cell lineage associated with human gastric adenocarcinoma. *Lab Invest* 1999;79:639–646.
  21. Correa P, Piazuelo MB. The gastric precancerous cascade. *J Dig Dis* 2012;13:2–9.
  22. Petersen CP, Weis VG, Nam KT, et al. Macrophages promote progression of spasmolytic polypeptide-expressing metaplasia after acute loss of parietal cells. *Gastroenterology* 2014;146:1727–1738. e8.
  23. Meyer AR, Engevik AC, Madorsky T, et al. Group 2 innate lymphoid cells coordinate damage response in the stomach. *Gastroenterology* 2020;159:2077–2091. e8.
  24. Vannucchi MG, Traini C, Manetti M, et al. Telocytes express PDGFRalpha in the human gastrointestinal tract. *J Cell Mol Med* 2013;17:1099–1108.
  25. Roth KA, Kapadia SB, Martin SM, et al. Cellular immune responses are essential for the development of *Helicobacter felis*-associated gastric pathology. *J Immunol* 1999;163:1490–1497.
  26. Nomura S, Yamaguchi H, Ogawa M, et al. Alterations in gastric mucosal lineages induced by acute oxyntic atrophy in wild-type and gastrin-deficient mice. *Am J Physiol Gastrointest Liver Physiol* 2005;288:G362–G375.
  27. Choi E, Hendley AM, Bailey JM, et al. Expression of activated Ras in gastric chief cells of mice leads to the full spectrum of metaplastic lineage transitions. *Gastroenterology* 2016;150:918–930. e13.
  28. McCarthy N, Manieri E, Storm EE, et al. Distinct mesenchymal cell populations generate the essential intestinal BMP signaling gradient. *Cell Stem Cell* 2020; 26:391–402. e5.
  29. Manieri E, Tie G, Malagola E, et al. Role of PDGFRA(+) cells and a CD55(+) PDGFRA(Lo) fraction in the gastric mesenchymal niche. *Nat Commun* 2023;14:7978.
  30. Lee SH, Contreras Panta EW, Gibbs D, et al. Apposition of fibroblasts with metaplastic gastric cells promotes dysplastic transition. *Gastroenterology* 2023; 165:374–390.
  31. Yum MK, Han S, Fink J, et al. Tracing oncogene-driven remodelling of the intestinal stem cell niche. *Nature* 2021;594, 442–427.

---

Received September 16, 2023. Accepted April 16, 2024.

#### Correspondence

Address correspondence to: James R. Goldenring, MD, PhD, Epithelial Biology Center, Vanderbilt University Medical Center, MRB IV 10435G, 2213 Garland Avenue, Nashville, Tennessee 37232-2733. e-mail: jim.goldenring@vumc.org.

#### Acknowledgements

The authors thank Dr Brenda Jarvis (Department of Cell and Developmental Biology, Vanderbilt University) for her valuable input in troubleshooting the TSA immunofluorescence protocol, and Dr Izumi Kaji (Department of Surgery, Vanderbilt University Medical Center) for sharing her tissue sample for the RNAscope protocol.

#### CRedit Authorship Contributions

Yoojin Sohn (Conceptualization: Equal; Data curation: Lead; Formal analysis: Lead; Investigation: Equal; Methodology: Equal; Validation: Lead; Visualization: Lead; Writing – original draft: Lead)

Blake Flores Semyonov (Data curation: Supporting; Investigation: Supporting; Visualization: Supporting; Writing – review & editing: Supporting)  
Hilana El-Mekkoussi (Investigation: Supporting; Methodology: Supporting; Visualization: Supporting; Writing – review & editing: Supporting)

Christopher V.E. Wright (Methodology: Supporting; Resources: Equal; Writing – review & editing: Supporting)

Klaus H. Kaestner (Conceptualization: Supporting; Methodology: Supporting; Resources: Equal; Writing – review & editing: Supporting)

Eunyoung Choi (Conceptualization: Supporting; Funding acquisition: Supporting; Methodology: Equal; Project administration: Supporting; Resources: Supporting; Writing – review & editing: Supporting)

James R. Goldenring, MD, PhD (Conceptualization: Equal; Funding acquisition: Lead; Investigation: Equal; Project administration: Lead; Resources: Lead; Supervision: Lead; Writing – review & editing: Equal)

**Conflicts of interest**

The authors disclose no conflicts.

**Funding**

Klaus H. Kaestner was supported by NIH R37 DK053839 and R01 DK139049. Eunyong Choi was supported by grants from NIH R37 CA244970 and NCI

R01 CA272687, and an AGA Research Foundation Funderburg Award (AGA2022-32-01). James R. Goldenring was supported by grants from a Department of Veterans Affairs Merit Review Award IBX000930, DOD CA190172, and NIH R01 DK101332 and NCI R01 CA272687. The Vanderbilt Cell Imaging Shared Resource is supported by the Vanderbilt Ingram Cancer Center (P30 CA068485) and the Vanderbilt Digestive Disease Research Center (P30 DK058404). The Translational Pathology Shared Resource is supported by NCI/NIH Cancer Center Support Grant (P30 CA68485) and The Shared Instrumentation Grant S10 OD023475-01A1 for the Leica Bond RX.